Monitoring CO emissions of the metropolis Mexico City using TROPOMI CO observations

Tobias Borsdorff[1], Agustín García Reynoso[2], Gilberto Maldonado[2], Bertha Mar-Morales[2], Wolfgang Stremme[2], Michel Grutter[2], and Jochen Landgraf[1]

[1]Netherlands Institute for Space Research, SRON, Utrecht, the Netherlands
[2]Centro de Ciencias de la Atmósfera, Universidad Nacional Autónoma de México, México City, Mexíco

Correspondence: T. Borsdorff (t.borsdorff@sron.nl)

Abstract. The Tropospheric Monitoring Instrument (TROPOMI) on ESA Copernicus Sentinel-5 satellite (S5-P) measures the carbon monoxide (CO) total column concentration as one of its primary targets. In this study, we analyse 551 TROPOMI overpasses over Mexico City (more than 2 years of measurements) using collocated CO simulations of the regional Weather Research and Forecasting (WRF) model to conclude on the emissions from different urban districts in the region. The WRF
5 simulation distinguishes the CO emissions from Tula, Pachuca, Tulancingo, Toluca, Cuernavaca, Cuautla, Tlaxcala, Puebla, the metropolian area of Mexico City (CDMX), and the adjoint urban area (ACDMX, CDMX surrounding municipalities from estate of Mexico) by 10 separate tracers. Using a regularised source inversion approach, the TROPOMI observations yields 0.10 Tg/yr and 0.08 Tg/yr CO emissions from the Tula and Pachuca urban areas in the North of Mexico city. This exceeds significantly the "Inventario Nacional de Emisiones de Contaminantes Criterio" (INEM) inventory that was adapted to the period
10 2017-2019 and results in an emissions <0.008 Tg/yr for both areas. For CDMX, TROPOMI estimates emissions of 0.14 Tg/yr CO, which is about half of the INEM emissions of 0.25 Tg/yr. ACDMX area, however, has a higher emissions with 0.29 Tg/yr according to TROPOMI observations versus 0.14 Tg/yr as stated by the INEM inventory. The total emission of both districts is similar (0.43 Tg/yr TROPOMI versus 0.39 Tg/yr adapted INEM emissions). Moreover, we found that the TROPOMI emission estimates for CDMX and ACDMX follow a clear weakly cycle with a minimum during the weekend. This agrees well with
15 ground-based in situ measurements from the "Secretaria del Medio Ambiente" (SEDEMA) and Fourier Transform Spectrometer column measurements in Mexico City that is operated by the Network for the detection of Atmospheric Composition Change Infrared Working Group (NDACC-IRWG). The study shows an approach to use the large amount of TROPOMI CO data to conclude on urban emissions on sub-city scales for metropolises like Mexico City but also indicates the clear need for further improvements of regional models like WRF, in particular with respect to the prediction of the local wind fields.

20 # 1 Introduction

Carbon monoxide (CO) is an atmospheric trace gas emitted by incomplete combustion to the atmosphere (e.g. biomass burning, industrial activity, and traffic). Its background concentration is relatively low with an atmospheric residence time varying from days to month (Holloway et al., 2000) depending on the atmospheric concentration of the hydroxyl radical (Spivakovsky et al.,

2000). These characteristics established CO as a tracer for air pollution and its transport in the atmosphere (e.g. (Gloudemans et al., 2009; Pommier et al., 2013; Schneising et al., 2019)).

The Tropospheric Monitoring Instrument (TROPOMI) launched 2017 as single payload of ESA's Copernicus Sentinel-5 Precursor mission aims on CO as one of its primary targets. The operational CO column product is inferred from TROPOMI's

5 shortwave infrared measurements with daily global coverage and a high spatial resolution of 7x7 km (Veefkind et al., 2012). Early in the mission, the TROPOMI CO dataset was validated with ground-based measurements of the Total Carbon Column Observing Network (TCCON) (Borsdorff et al., 2018a), and inter-compared with the simulated CO fields of the European Centre for Medium-Range Weather Forecasts (ECMWF) - Integrated Forecasting System (Borsdorff et al., 2018b). On 11 July 2018, it was concluded that the TROPOMI CO data quality is fully compliant with the mission requirements of 15% precision

10 and 10% accuracy and so it was released for public usage (https://scihub.copernicus.eu).

Borsdorff et al. (2018a, 2019) illustrated the capability of TROPOMI to detect CO emissions from pollution hot spots of medium size to large cites (e.g. Yerevan, Tabriz, Urmia, and Tehran), industrial areas (e.g. Po valley in Italy), and even pollution along arterial roads in Armenia. To monitor the emissions of metropolises, data interpretation of multi-annual data sets is required. The different inversion techniques discussed by (Varon et al., 2018) for plume inversions, i.e. the source pixel

15 method, the mass balance method and the inversion of a Gaussian plume model are appropriate to interpret emission of point sources but are less suitable for flux inversion of spatially extended sources. Therefore, in this study we estimate CO emission inverting the regional atmospheric modeling Weather Research and Forecasting (WRF) as an atmospheric tracer transport model, which allows to simulate the CO column on the spatial resolution as TROPOMI. Possible error sources of this type of flux inversion is the limited validity of the simulated wind fields, prior assumption on the spatial distribution of emissions, and

20 the simulated atmospheric dispersion.

Mexico City is a prime example of a CO pollution hot spot that is clearly detectable by TROPOMI. It is a fast growing mega city located at an altitude of 2240 m on the Central Plateau which is surrounded by mountains. The urban area is divided in ten different urban districts (Tula, Pachuca, Tulancingo, Toluca, CDMX, Cuernavaca, Cuautla, Tlaxcala, Puebla, CDMX, and ACDMX) and the metropolis has a long history of atmospheric pollution measurements. More than 29 in situ CO measurements

25 stations are distributed over the city operated by the "Secretaria del Medio Ambiente" (SEDEMA, Mexican Ministry of the Enviroment). About every 2 years, the ministry reports on the CO emission of Mexico City. Based on the bottom-up approach using the in situ measurements, it is concluded that a major part of Mexico City's CO emission is caused by light duty motor vehicles. SEDEMA found a decline of the CO emissions for the Zona metropolitana del valle de Mexico (ZMVM) from 2.04 Tg/yr in 2000, 0.7 Tg/yr in 2014, to 0.28 Tg/yr in 2016 SMA-GDF (2018). Here the emission estimation changed by 0.42 Tg/yr

30 in only 2 years from 2014 to 2016, due to a change in the mobile emission model from 'mobile' to 'moves'. The emission estimate for the total central area wich is 0.73 Tg/yr for the year 2016 splits up into 0.28 Tg/yr for CDMX, 0.43 Tg/yr for ACDMX, and 0.02 Tg/yr for Tizayuca.

Moreover, ground-based FTIR measurements are regularly performed as part of the NDACC (Network for the detection of Atmospheric Composition Change) - IRWG (Infrared Working Group), which provide CO total column concentrations. Using

35 these measurements and IASI satellite observations of CO, Stremme et al. (2013) estimated the overall annual CO emission

of Mexico City to be about 2.15 Tg/yr for the year 2008. TROPOMI CO observations add new possibilities for air quality monitoring due to the regional coverage, the daily overpass combined with the high precision of the data.

In this study, we analyse more than 2 years of TROPOMI CO measurements using collocated WRF CO simulations for Mexico to get more insight into the emission of Mexico City. Section 1 introduces the TROPOMI CO dataset and the simulation

5   of the WRF model. Section 2 describes our methodology to fit the WRF model to the TROPOMI data for emission estimates. Sections 3 discusses our finding and section 4 gives the summary and conclusion.

2   TROPOMI CO data set

This study uses the TROPOMI dataset of CO total column concentration between 14th November 2017 and 25th August 2019 over Mexico. On 5 August, 2019, the spatial sampling of the data product at satellite nadir geometry was improved from

10   7x7 km^2 to 7x5.6 km^2 due to a shorter readout time of the detectors. The data processing deploys the shortwave infrared CO retrieval (SICOR) algorithm that was developed for the Copernicus operational data processing (Landgraf et al., 2016a). Algorithm settings like the spectral windows, priori profiles and auxiliary are introduced in (Landgraf et al., 2016b). The retrieval utilizes an forward calculation accounting for atmospheric scattering that allows to retrieve effective cloud parameters (altitude, optical thickness) together with the total column concentrations of CO and of the interfering gases H_2O, HDO and

15   CH_4 (Vidot et al., 2012). The forward calculation uses the HITRAN 2016 database for all species as described by (Borsdorff et al., 2019) and the inversion deploys profile scaling approach that scales a reference profile to fit the spectral measurement (Borsdorff et al., 2014). Here, the priori profile is taken from a spatio-temporally resolved atmospheric transport simulations of the TM5 model (Krol et al., 2005). The TROPOMI data product also provides the total column averaging kernel a_{col} that relates the real vertical CO profile ρ_{true} to the retrieved total column concentration c_{ret} following the equation

20 $$c_{ret} = a_{col}\rho_{true} + \epsilon \tag{1}$$

with the noise contribution ϵ. In this study we limit our analysis to scenes under clear-sky and low-cloud atmospheric conditions, which corresponds to the filtering of quality assurance value $q > 0.5$. Individual TROPOMI CO orbits show an artificial striping in flight direction, probably due to calibration inaccuracies. For de-striping, we apply an a posteriori correction to the retrieved CO columns as discussed in (Borsdorff et al., 2019) based on frequency filtering in the Fourier space.

25   3   Methodology

3.1   The WRF model

We simulate the CO column concentrations measured by TROPOMI by deploying the WRF-Chem model version 3.9.1.1. The simulation covers the time period of TROPOMI measurements on the regional domain shown in Fig. 1. It assumes a time invariant CO background concentration and does not account for atmospheric chemistry (Dekker et al., 2017). The spatial

30   resolution of the simulation is chosen to be comparable with the TROPOMI CO product sampling. Each grid cell of the

considered simulation domain ($270\text{x}270\text{km}^2$) is $3\text{x}3\text{k}^2$. The WRF simulation employs the emission inventory "Inventario Nacional de Emisiones de Contaminantes Criterio" (INEM) for the year 2013 but scaled by a factor of 0.48 to make it applicable for the years 2017 to 2019. This factor was obtained when comparing the model results against surface measurements (García-Reynoso et al., 2018). The inventory is time dependent and accounts for the diurnal, week-to-week and monthly variations of

5   the emissions. Moreover, the model run is constraint by NCEP North American Mesoscale (NAM) 12 km analysis wind fields (NCEP, 2015). Finally, WRF yields vertical CO concentration profiles for every latitude/longitude grid cell and every model time step and tracer run. To estimate different CO emissions areas in central Mexico, the WRF simulation uses ten independent tracer, one for Tula, Pachuca, Tulancingo, Toluca, Cuernavaca, Cuautla, Tlaxcala, Puebla, the metropolian area of Mexico City (CDMX), and the adjoint urban area (ACDMX). Hence, the total simulated CO field is given by the sum of the simulated CO

10 fields of the tracer together with the spatiotemporal constant CO background. Since no atmospheric chemistry is accounted, the CO tracer field is linear in a scaling α_i of the corresponding emissions per district,

$$\mathbf{F}_{\text{WRF}}(\alpha_1, \cdots, \alpha_{10}, \alpha_{\text{bg}}) = \sum_{i=1}^{10} \mathbf{k}_i \alpha_i + \mathbf{k}_{\text{bg}} \alpha_{\text{bg}} \tag{2}$$

where $\mathbf{k}_i$ represents the CO tracer field for the reference emission (adapted INEM data) for $\alpha_i = 1$. Further, the forward model assumes linear dependence of CO background field $\mathbf{k}_{\text{bg}}$ with scaling parameter α_{bg} (Borsdorff et al., 2019).

15 Before contrasting the model simulations with the observations, we first interpolate the model fields to the geolocation and time of the TROPOMI observations and second integrate the model CO profiles to total column densities by applying the total column averaging kernel of the TROPOMI CO retrieval following equation 2. We summarize this numerical step in the observation operator $\mathcal{O}$, which transforms the forward model into

$$\mathbf{F}_{\text{sat}}(\alpha_1, \cdots, \alpha_{10}, \alpha_{\text{bg}}) = \sum_{i=1}^{10} \mathcal{O}(\mathbf{k}_i) \alpha_i + \mathbf{k}_{\text{bg}} \alpha_{\text{bg}} \tag{3}$$

20 Hence, the operator $\mathcal{O}$ accounts for the TROPOMI specific vertical sensitivity, which can change from measurement to measurement and so ensures that the comparison between TROPOMI and WRF is free of the null-space or smoothing error (Rodgers, 2000; Borsdorff et al., 2014). Here the scaling factors α_i per emission area are not affected by the operation.

In a next step, we transform Eq. (3) to

$$\mathbf{F}_{\text{sat}}(E_1, \cdots, E_{10}, \alpha_{\text{bg}}) = \sum_{i=1}^{10} \mathcal{O}(\tilde{\mathbf{k}}_i) E_i + \mathbf{k}_{\text{bg}} \alpha_{\text{bg}} \tag{4}$$

25 Here, $\tilde{\mathbf{k}}_i = \frac{\mathbf{k}_i}{E_{i,INEM}}$ and $E_i = \alpha_i E_{i,INEM}$ with the corresponding emissions $E_{i,INEM}$ of the INEM inventory interpolated to the TROPOMI overpass time.)

Finally, to improve the capability of the forward model to fit TROPOMI observations, we induce a linear altitude dependence of the simulated CO column $\mathbf{k}_{\text{elv}} = z - z_{\text{ref}}$. Here, z is the mean elevation in the TROPOMI CO ground pixels and $z_{\text{ref}} = 2240$ m the reference altitude which is set to the elevation of Mexico City.

30 $$\mathbf{F}_{\text{sat}}(E_1, \cdots, E_{10}, \alpha_{\text{bg}}) = \sum_{i=1}^{10} \mathcal{O}(\tilde{\mathbf{k}}_i) E_i + \mathbf{k}_{\text{bg}} \alpha_{\text{bg}} + \mathbf{k}_{\text{elv}} \alpha_{\text{elv}} \tag{5}$$

With this additional degrees of freedom the forward model can mitigate shortcomings of the WRF simulations using a spatially constant CO background.

In our simulation of TROPOMI CO observations, we assume that the local enhancements of CO are due to emissions of the city districts of the same day, whereas emissions from outside the domain as well as the temporal accumulation of CO emission of the domain is described by the background CO field. Therefore, it means that the inferred emissions E_i represents an emission estimate of the urban district for the particular observation day. Moreover, the effective model parameter α_{bg} and α_{elv} may vary between different TROPOMI overpasses.

3.2 Inversion

The linear forward model in Eq. (5) can be written in a matrix-vector notation,

$$F_{\mathrm{sat}}(\mathbf{x}) = \mathbf{K}x \tag{6}$$

with the state vector $\mathbf{x} = (E_1, \cdots, E_{10}, \alpha_{\mathrm{bg}}, \alpha_{\mathrm{elv}})$ and the corresponding forward model Jacobian $\mathbf{K} = (\tilde{\mathbf{k}}_1, \cdots \tilde{\mathbf{k}}_{10}, \mathbf{k}_{\mathrm{bg}}, \mathbf{k}_{\mathrm{elv}})$.

To fit our forward model to the observations $\mathbf{y}_{meas}$ of a single TROPOMI overpass, we use the regularized least-squares fit as described by Rodgers (2000).

$$\mathbf{x}_{\mathrm{ret}} = \min_{\mathbf{x}} \left\{ ||\mathbf{y}_{\mathrm{meas}} - \mathbf{K}\mathbf{x}||^2_{S_e} - ||\mathbf{x} - \mathbf{x}_a||^2_{\Gamma} \right\} \tag{7}$$

The norms are defined by $||p||^2_M = p^T \cdot M^{-1} p$ for a vector p and a matrix M. Vector $\mathbf{x}_{\mathrm{ret}}$ is the estimated state vector and $\mathbf{x}_a$ is a priori estimate. Here, $\mathbf{S}_e$ is the measurement error covariance matrix given by the TROPOMI retrieval error on the diagonal and Γ the regularization matrix which is in our case diagonal too.

The solution of the minimization problem (Eq. 3.2) is given by

$$\mathbf{x}_{ret} = \mathbf{G}(\mathbf{y}_{\mathrm{meas}} - \mathbf{K}\mathbf{x}_a) + \mathbf{x}_a \tag{8}$$

with the gain matrix

$$\mathbf{G} = (\mathbf{K}^T \mathbf{S}_e^{-1} \mathbf{K} + \Gamma)^{-1} \mathbf{K}^T \mathbf{S}_e^{-1} \tag{9}$$

The averaging kernel relates the 'true' state vector $\mathbf{x}_{\mathrm{true}}$ to $\mathbf{x}_{\mathrm{ret}}$, namely

$$\mathbf{x}_{\mathrm{ret}} = \mathbf{A}\left(\mathbf{x}_{\mathrm{true}} - \mathbf{x}\right) + \mathbf{x}_a \tag{10}$$

with

$$\mathbf{A} = \mathbf{G}\mathbf{K} \tag{11}$$

$\mathbf{A}$ represents the derivative $\mathbf{A}_{ij} = \frac{\partial x_{ret,i}}{\partial x_{true,j}}$, where its diagonal elements describe the retrieval sensitivity of a state vector element to its true value. The degree of freedom for signal

$$\mathrm{DFS} = \mathrm{trace}(\mathbf{A}), \tag{12}$$

indicates the total number of independent pieces of information.

To evaluate the fit quality for each overpass, we consider the fit residuals $\delta_j = \mathbf{y}_{\mathrm{meas},j} - F_j(\mathbf{x})$ with j subscribing each individual observation of an overpass. Here, $F(\mathbf{x})$ represents the measurement simulation after fitting. This yields the mean

$$\langle \delta \rangle = \frac{1}{J} \sum_{j=1}^{J} \delta_j \qquad (13)$$

5   and the standard deviations of the residuals

$$\sigma(\delta) = \frac{1}{J-1} \sum_{j=1}^{J} (\delta_i - \langle \delta \rangle)^2 \qquad (14)$$

The standard deviation $\sigma(\mathbf{y}_{\mathrm{meas}})$ and $\sigma(\mathbf{F}(\mathbf{x}))$ of the TROPOMI CO field and the corresponding WRF forward simulation completes our set of diagnostics.

Applying the regularization the retrieved emissions are constrained to a certain prior state $\mathbf{x}_a$, which can induce an overall
10   bias to the data product if the prior is not chosen carefully.

3.3   Pre-fit

In a pre-fit step we determine the prior emissions from a set of TROPOMI data with highest information content, such that the emissions can be inferred without any regularization, $\Gamma = 0$. Here, individual emission estimates may be noisy due to non-optimized noise propagation in the inversion, however, averaging all inversions reduces noise contribution and so gives a
15   reliable estimate of a mean emission for the different districts. The validity of this approach depends crucially on the selected data set of TROPOMI overpasses. On one hand, it should be large enough to estimate mean emissions for the period of TROPOMI observations, and the other hand strict data filtering is required to get a stable inversion with little forward model errors.

The information content of a single overpass varies and depends on several aspects: (1) The number of useful measurements
20   and their cloud coverage changes between different TROPOMI overpasses. Here, clouds shield the lower troposphere, where atmospheric measurements are particular sensitive to the surface emissions E_i. (2) The pixel size at the swath edge is about 32 km and so about 5 times larger than at the sub-satellite point. This reduces not only the number of pixels covering a certain area but also the sensitivity of the individual TROPOMI observations. (3) The quality of the forward model depends on the meteorological situation, where we consider model simulations for low wind speeds more reliable. This considerations led to
25   the criteria of the data filtering for the pre-fit. Thus, we only select overpasses which meet all of following filter criteria:

- 70 % of the data domain is covered by TROPOMI observations

- for all observations the across track pixel size is < 15 km.

- the average wind speed of the scene is < 4 m/s.

- The fit residuum $\langle \delta \rangle < 8$ppb, and the standard deviation $\sigma(\delta) < 8$ppb to limit the effect of too large forward model
30   errors.

- $\sigma(\delta)/\delta(\mathbf{y}_{\text{meas}}) < 0.65$ to ensure that the forward model can explain the variability of the measured CO field.

- $\sigma(\mathbf{F}(\mathbf{x})) > 4$ ppb to ensure that the model data contain a clear pollution signatures.

- the Pearson correlation coefficient $r > 0.3$ between $CO_{TROPOMI}$ and CO_{WRF}.

The filter criteria reduce the original set of 551 overpasses to 148, which we consider to be sufficient to estimate the overall average emission rate per district, yielding the prior state vector $\mathbf{x}_a$. For this we use the median instead of the mean because of its robustness against outliers. With the same reasoning we define the percentile difference

$$\delta P_j = |\frac{P_j(84.1) - P_j(15.9)}{2}| \tag{15}$$

, to describe scattering in the data, which corresponds to the standard deviation of normal distributed parameters. Finally, we calculate the error of the mean using the percentile difference.

3.4 Final-fit

Subsequently, the final data reduction steps is performed. To reduce the noise propagation in the inversion and to become independent on the prior data selection, we regularize the inversion to the prior state determined by the pre-fit. Here, we choose Γ to be a diagonal matrix with

$$\mathrm{d}iag\Gamma = [\gamma_1, \gamma_2, \cdots, \gamma_{10}, 0, 0] \tag{16}$$

such that the elements of the state vector $\alpha_{\text{b}g}$ and α_{elv} are not regularized. Obviously, the regularization parameter γ_i must be well-chosen to optimize the balance between minimum error propagation on the fit parameter and maximum information content inferred from the measurement. If γ_i is chosen too small, the propagation of the TROPOMI measurement noise as well as retrieval biases and forward model errors dominates the inversion. If γ_i is chosen too large, the estimated state vector reproduces the prior estimate without appropriate use the information content of the measurement. For our application, we fix the regularization parameter γ_i for $i = 1, \cdots, 10$ to constant values such that the scatter of the retrieved emissions stays within predefined boundaries. Considering the temporal variation of the INEM emissions to be about 40%, we adjusted the regularization parameter $\gamma_1, \cdots, \gamma_{10}$ such that the retrieved emissions vary with 60% around their average. This puts a moderate constraints on the inversion ensuring on one hand a stable inversion and on the other hand a realistic variation of the retrieved emissions around the priori.

A great advantage of the Final-fit compared to the Pre-fit is that the retrieved emissions can be filtered with respect to the information provided by the TROPOMI measurements. We filter on the information for each tracer emission E_i individually, considering inferred emissions with $(AK(i,i) > 0.3)$. This form of data mining optimizes the data use, keeping in mind that TROPOMI overpasses may be appropriate to determine one specific source but not all sources simultaneously. In this manner, noise propagation in the inversion can be minimized. This concept of information content based filtering turned out to be very useful. The filter criteria of the Pre-fit are not required anymore for the Final-fit to achieve a very similar performance. A filtering like this is not possible for the Pre-fit since the averaging kernel of an regularized retrieval is by definition $(AK(i,i) = 1)$.

4 Results

Fig. 2 shows the fitted CO background concentration and its annual cycle. Here, the biomass burning season between February and June causes the corresponding CO enhancement, whereas lower CO concentrations are observed during the rain season between June and November. The extremely high CO column values on the 15th May 2019 are due to the transport of CO

5   enriched air from wild fires in the South-West of Mexico in to the model domain. Figure 3 shows the CO concentration in the state of Mexico under normal conditions and after the fires, which caused a serious health hazard in Mexico City. These type of fires outside the model domain create an inhomogeneous background CO field over Mexico City, which cannot be described by our forward model. Only fitting a scaling to a constant background field is not sufficient in this extreme cases and so during the fire season many data cannot be considered.

10   Figure 4 shows three examples of TROPOMI overpasses, which includes a pixel resolution of 7x7 km^2 (panel (a), (b), and (c)) and the enhanced spatial resolution of 7x5.6 km^2 (panel (d)), where latter is the TROPOMI instrument baseline since the 6th of August 2019. Focusing on the dry season, the TROPOMI instrument can detect distinct CO enhancements over the different emission areas in Central Mexico with the retrievals from single orbit overpasses (see left column of Fig. 4). After fitting our forward model to the TROPOMI measurements, as part of the Final-fit, brings simulated data and observations into

15   good agreement as illustrated in Fig. 4. Particular for low wind speed conditions in Fig. 4(a), TROPOMI and WRF show distinct CO enhancements over the different emission areas of Mexico. Furthermore, the transport of CO enhanced air form Mexico City towards the South following the mountain orography and the accumulation of CO in the South is seen by TROPOMI in agreement with the WRF simulation (4(c). This clearly shows that regional models like WRF have a great potential for the interpretation and analysis of TROPOMI data. However, we also found clear localized residuals in the difference δ_j between

20   observations and forward model. (right column of Fig. 4). For atmospheric conditions under high wind speeds the WRF simulations can deviate more from the TROPOMI measurements as shown in Fig. 4 (c). Here, the plume of CO enriched air extending from Mexico City towards the North is simulated very narrow compared to the more dispersed plume seen by TROPOMI. This points to an possible underestimation of the atmospheric dispersion in the WRF simulation. A very prominent residual between TROPOMI and WRF is shown in 4 (d) but also present in 4 (a) and (b). Here TROPOMI measures a strong

25   CO enhancement in the North of Mexico City that is not reproduced by the WRF model. This points at a deficient spatial distribution of INEM emissions.

Fig. 5 (a) shows for each tracer doamin the averaged emissions of the Final-fit derived from the TROPOMI data E_i in comparison to the ones of the Pre-Fit and the priori emission used for the WRF simulation (adapted INEM inventory). We find significant differences between the emissions of the priori and the Final-fit. The retrieved emissions of the Final-fit from

30   the urban districts Tula (0.10 Tg/yr) and Pachuca (0.08 Tg/yr) in the North of Mexico city seem to be underestimated by the emission inventory (both were less then 0.008 Tg/yr). Furthermore we found that the emission of the central part of Mexico city (CDMX) is assumed too high in the priori emissions (0.25 Tg/yr). The TROPOMI measurements indicate lower values for CDMX (0.14 Tg/yr) which come along with higher values for the district ACDMX (0.29 Tg/yr). The sum of both emissions (0.43 Tg/yr) is similar to the priori emissions (0.39 Tg/yr). This may mean that the total emissions of the domain including

CDMX and ACDMX is well represented in the emission inventory but only the spatial distribution of the source intensity is unrealistic.

In General, the retrieved emissions of the Final-fit are in good agreement with the one of the Pre-fit. The explanation for this is simple, the retrieved emission of the Pre-fit are used as priori for the regularized inversion of the Final-fit as described in

5 Sec 3.4. The scatter of the individual retrievals of the Pre-fit is high and in most cases exceeds 100% (see Fig. 5 (b)). This is most probably caused by forward model errors as discussed before. Furthermore, non-uniform variation of the background CO concentration can be a additional reason for this scatter (as shown in Fig. 3). However, the average of the individual retrievals of the Pre-fit is more trustworthy (see error bars in Fig. 5 (a)) and by that is our best estimate of an unbiased emission priori for the Final fit. The regularization of the Final-Fit succeeds to reduce the scatter of the individual retrieval as shown in 5 (b)).

10 In Fig. 6, the averaging kernel of the examples cases shows high values on the diagonal indicating that the Final-fit even using the regularization can distinguish emissions of the different urban districts of Mexico. Moreover, the averaging kernel shows that the Final-fit inversion is insensitive to deviations of the Tulancingo emission from the prior estimate. Whereas the Pre-fit inversion estimates very small emissions for this district, the subsequent regularization changes the emission only marginally. Furthermore, the regularization of the Final-fit imposes cross-correlations e.g. between CDMX and ACDMX as

15 can be seen in panel (d) of Fig. 6, which are still small compared the diagonal. In general, for a correct interpretation of the retrieved emissions the averaging kernels shown in Fig. 6 needs to be taken in account when ever possible. So, one can filter the emission product with respect to the information provided by the TROPOMI measurements. Hence, for the Final-fit, we filter on the information for each tracer emission E_i individually. This results in different number of coincidences for the different districts (panel (c) of Fig 5). This form of data mining optimizes the data use, keeping in mind that TROPOMI overpasses may

20 be appropriate to determine one specific source but not all sources simultaneously. In this manner, noise propagation in the inversion can be minimized.

Due to the reduced scatter and the higher data amount of the Final-fit for the suburbs CDMX and ACDMX, the Final-fit allows to conclude on the time dependent variability of emission in Mexico City. Figure 7 (a) shows the time series of the emission for CDMX and ACDMX, which vary around the priori value. This temporal variation is determined from the

25 measurements as all prior information is assumed to be time invariant. Panel (b) of the figure shows relatively high values of the diagonal elements of the averaging kernel for the emissions of the two urban districts. Finally, panel (c) of the figure indicates a clear weakly CO cycle in the data with low values during weekends. During the week the CO emissions of the two districts do not differ significantly due to the error estimates and more TROPOMI data is required to further constrain the weekly cycle.

30 A similar weakly cycle is observed by Mexico City situ measurements provided by 29 SEDEMA ground stations. For each of the sites, we use data from 2017 to 2018 for the overpass time of TROPOMI (12h-15h local time), calculated an weakly cycle and group the data in the stations located in the CDMX urban area and those located in the wider area of the metropolis. Figure 8a depicts the median of all weakly cycles and the standard error of the mean with a clear minimum during weekends. The error bars indicate that the overall shape of the weekly cycles for the remaining days vary a lot from station to station.

The lower CO concentrations during the weekend are also detectable with column retrievals from ground-based FTIR measurements in Mexico City 2280 m.a.s.l 19.32°N and -99.18°E at the campus of the national University by the atmospheric science center (CCA). The used spectra are recorded in the mid infrared with a resolution of 0.075 cm^{-1} (Bezanilla et al., 2014; Plaza-Medina et al., 2017) and the CO column and profile is retrieved using the standard NDACC retrieval strategy (García-Franco et al., 2018; Borsdorff et al., 2018a). Figure 8b shows the averaged weakly cycle with standard error derived from the column measurements. Due to the low data density at weekends we used the full time range from the 5th December 2010 to the 10th September 2019 without filtering for the overpass time of TROPOMI. These independent ground based measurements confirm the weekly CO cycle found in the TROPOMI data.

5 Conclusions

In this study, we analyzed TROPOMI CO retrieval from 551 overpasses of the instrument over Central Mexico, which corresponds to about 2-years of measurements starting from the 14th November 2017 until the 25th August 2019. We found that the TROPOMI CO data allows pollution monitoring by single overpasses with a high spatial resolution of 7x7 km^2 that is enhanced to 7x5.6 km^2 from the 6th of August 2019 onwards. The high signal-to-noise ratio of the measurements allows to distinguish distinct CO enhancements over the various urban districts of Central Mexico using single orbit overpasses of TROPOMI.

With a dedicated WRF tracer simulation for the full time range of the current TROPOMI data record, we could distinguish the contribution of ten urban districts Tula, Pachuca, Tulancingo, Toluca, Cuernavaca, Cuautla, Tlaxcala, Puebla, CDMX, and ACDMX. The model data was collocated with the TROPOMI measurements and convolved with the total column averaging kernel to account for the vertical sensitivity of the instrument. The WRF tracer simulation does not account for atmospheric chemistry and so the simulated CO tracer fields is linear in the emission rates of the different districts.

The CO emissions are determined in two steps. First we apply a unregularized least squares fit of the model to the TROPOMI observations to determine the averaged emission per district. A strict data screening based on the measurements and WRF model simulation reduced the TROPOMI data set from 551 to 148 overpasses. For this data set, the fit quality is good after introducing two auxiliary fit parameters for the background variability with time and the dependency of the simulated column on terrain height. However, the individual emission rates show a high scatter exceeding 100% of the averaged emissions. When averaging the filtered emissions, the averaged emissions for the various urban districts of Mexico deviates from emission estimates of the "Inventario Nacional de Emissions de Contaminantes Criterio" (INEM) inventory adapted to the period 2017-2019. The TROPOMI emissions from the urban districts Tula (0.10 Tg/yr) and Pachuca (0.08 Tg/yr) in the Norther of Mexico city deviate significantly from the INEM inventory with 0.008 Tg/yr for both areas. For the emission of the central part of Mexico city (CDMX), TROPOMI indicate 0.14 Tg/yr versus 0.25 Tg/yr INEM emissions and 0.29 Tg/yr versus 0.14 Tg/yr INMEN emissions for the district ACDMX. Together, both districts have similar emissions with 0.43 Tg/yr seen by TROPOMI versus 0.39 Tg/yr from the inventory, pointing to a different relative distribution of the CO emissions seen by TROPOMI.

Finally, in a second retrieval, we regularize the inversion towards the mean emission estimate, determined in the first step. This reduces the scatter of the retrieved emissions to about 60% of the median for all urban districts. For data interpretation and

screening, the use of the averaging kernel is of great advantage. It allows to diagnose cross correlations between the inferred emission rates, which in general is weak for our application. Moreover, the a posteriori data screening uses the averaging kernel to optimize data selection per emission source. This filter concept is very powerful and allows us to distill from the data set a weakly cycle of CO emission at the districts CDMX and ACDMX with a clear minimum during weekends. This finding is in
5   agreement with in situ observations and ground-based FTIR measurement in the metropolis.

Our study shows the need and the potential of regional atmospheric transport modeling for the interpretation of TROPOMI CO data over metropolitan areas like Mexico City. Here, the CO pollution is a composite of emissions from different districts and its transport leads to complex CO enhancement patterns in the atmosphere. The WRF tracer model could simulate the TROPOMI measurement to a great extend, however model errors are still significant and further improvement is required to
10 fully explore the TROPOMI CO observations over mega-cities.

6   Data availability

The TROPOMI CO data set of this study is available for download at ftp://ftp.sron.nl/open-access-data-2/TROPOMI/tropomi/co/. The in situ measurements in Mexico City were downloaded from http://www.aire.cdmx.gob.mx. The ground-based FTIR measurements in Mexico can be downloaded http://www.epr.atmosfera.unam.mx/ftir_data/UNAM/CO/VERTEX/v1/.

15 *Author contributions.* Tobias Borsdorff, and Jochen Landgraf performed the TROPOMI CO retrieval and data analysis. Agustin Garcia Reynoso, Gilberto Maldonado, and Bertha Mar-Morales performed the WRF simulation. Wolfgang Stremme and Michel Grutter provided the ground-based FTIR measurements. All authors discussed the results and commented on the manuscript.

Competing interests. The authors declare no competing interests.

Disclaimer. The presented work has been performed in the frame of the Sentinel-5 Precursor Validation Team (S5PVT) or Level 1/Level 2
20 Product Working Group activities. Results are based on preliminary (not fully calibrated/validated) Sentinel-5 Precursor data that will still change. The results are based on S5P L1B version 1 data.

Acknowledgements. The presented material contains modified Copernicus data [2017,2018] The TROPOMI data processing was carried out on the Dutch national e-infrastructure with the support of the SURF Cooperative.

References

Bezanilla, A., Krüger, A., Stremme, W., and de la Mora, M. G.: Solar absorption infrared spectroscopic measurements over Mexico City: Methane enhancements, Atmósfera, 27, http://www.revistascca.unam.mx/atm/index.php/atm/article/view/43392, 2014.

Borsdorff, T., Hasekamp, O. P., Wassmann, A., and Landgraf, J.: Insights into Tikhonov regularization: application to trace gas column retrieval and the efficient calculation of total column averaging kernels, Atmospheric Measurement Techniques, 7, 523–535, https://doi.org/10.5194/amt-7-523-2014, https://doi.org/10.5194%2Famt-7-523-2014, 2014.

Borsdorff, T., aan de Brugh, J., Hu, H., Hasekamp, O., Sussmann, R., Rettinger, M., Hase, F., Gross, J., Schneider, M., Garcia, O., Stremme, W., Grutter, M., Feist, D. G., Arnold, S. G., De Mazière, M., Kumar Sha, M., Pollard, D. F., Kiel, M., Roehl, C., Wennberg, P. O., Toon, G. C., and Landgraf, J.: Mapping carbon monoxide pollution from space down to city scales with daily global coverage, Atmospheric Measurement Techniques Discussions, 2018, 1–19, https://doi.org/10.5194/amt-2018-132, https://www.atmos-meas-tech-discuss.net/amt-2018-132/, 2018a.

Borsdorff, T., de Brugh, J. A., Hu, H., Aben, I., Hasekamp, O., and Landgraf, J.: Measuring Carbon Monoxide With TROPOMI: First Results and a Comparison With ECMWF-IFS Analysis Data, Geophysical Research Letters, 45, 2826–2832, https://doi.org/10.1002/2018GL077045, https://agupubs.onlinelibrary.wiley.com/doi/abs/10.1002/2018GL077045, 2018b.

Borsdorff, T., aan de Brugh, J., Pandey, S., Hasekamp, O., Aben, I., Houweling, S., and Landgraf, J.: Carbon monoxide air pollution on sub-city scales and along arterial roads detected by the Tropospheric Monitoring Instrument, Atmospheric Chemistry and Physics, 19, 3579–3588, https://doi.org/10.5194/acp-19-3579-2019, https://www.atmos-chem-phys.net/19/3579/2019/, 2019.

Dekker, I. N., Houweling, S., Aben, I., Röckmann, T., Krol, M., Martínez-Alonso, S., Deeter, M. N., and Worden, H. M.: Quantification of CO emissions from the city of Madrid using MOPITT satellite retrievals and WRF simulations, Atmospheric Chemistry and Physics, 17, 14 675–14 694, https://doi.org/10.5194/acp-17-14675-2017, http://dx.doi.org/10.5194/acp-17-14675-2017, 2017.

García-Franco, J. L., Stremme, W., Bezanilla, A., Ruiz-Angulo, A., and Grutter, M.: Variability of the Mixed-Layer Height Over Mexico City, Boundary-Layer Meteorology, 167, 493–507, https://doi.org/10.1007/s10546-018-0334-x, https://doi.org/10.1007/s10546-018-0334-x, 2018.

García-Reynoso, J., Mar-Morales, B., and Ruiz-Suárez, L.: MODELO DE DISTRIBUCIÓN ESPACIAL, TEMPORAL Y DE ESPECIACIÓN DEL INVENTARIO DE EMISIONES DE MÉXICO (AÑO BASE 2008) PARA SU USO EN MODELIZACIÓN DE CALIDAD DEL AIRE (DiETE), Revista Internacional de Contaminación Ambiental, 34, 635–649, https://doi.org/10.20937/RICA.2018.34.04.07, https://www.revistascca.unam.mx/rica/index.php/rica/article/view/RICA.2018.34.04.07, 2018.

Gloudemans, A. M. S., de Laat, A. T. J., Schrijver, H., Aben, I., Meirink, J. F., and van der Werf, G. R.: SCIAMACHY CO over land and oceans: 2003–2007 interannual variability, Atmospheric Chemistry and Physics, 9, 3799–3813, https://doi.org/10.5194/acp-9-3799-2009, https://doi.org/10.5194%2Facp-9-3799-2009, 2009.

Holloway, T., Levy, H., and Kasibhatla, P.: Global distribution of carbon monoxide, Journal of Geophysical Research: Atmospheres, 105, 12 123–12 147, https://doi.org/10.1029/1999jd901173, https://doi.org/10.1029%2F1999jd901173, 2000.

Krol, M., Houweling, S., Bregman, B., van den Broek, M., Segers, A., van Velthoven, P., Peters, W., Dentener, F., and Bergamaschi, P.: The two-way nested global chemistry-transport zoom model TM5: algorithm and applications, Atmospheric Chemistry and Physics, 5, 417–432, https://doi.org/10.5194/acp-5-417-2005, https://www.atmos-chem-phys.net/5/417/2005/, 2005.

Landgraf, J., aan de Brugh, J., Borsdorff, T., Houweling, S., and O., H.: Algorithm Theoretical Baseline Document for Sentinel-5 Precursor: Carbon Monoxide Total Column Retrieval, Atbd, SRON, Sorbonnelaan 2, 3584 CA Utrecht, The Netherlands, 2016a.

Landgraf, J., aan de Brugh, J., Scheepmaker, R., Borsdorff, T., Hu, H., Houweling, S., Butz, A., Aben, I., and Hasekamp, O.: Carbon monoxide total column retrievals from TROPOMI shortwave infrared measurements, Atmospheric Measurement Techniques, 9, 4955–4975, https://doi.org/10.5194/amt-9-4955-2016, https://doi.org/10.5194%2Famt-9-4955-2016, 2016b.

NCEP: NCEP North American Mesoscale (NAM) 12 km Analysis, https://doi.org/10.5065/G4RC-1N91, 2015.

Plaza-Medina, E. F., Stremme, W., Bezanilla, A., Grutter, M., Schneider, M., Hase, F., and Blumenstock, T.: Ground-based remote sensing of O_3 by high- and medium-resolution FTIR spectrometers over the Mexico City basin, Atmospheric Measurement Techniques, 10, 2703–2725, https://doi.org/10.5194/amt-10-2703-2017, https://www.atmos-meas-tech.net/10/2703/2017/, 2017.

Pommier, M., McLinden, C. A., and Deeter, M.: Relative changes in CO emissions over megacities based on observations from space, Geophysical Research Letters, 40, 3766–3771, https://doi.org/10.1002/grl.50704, http://dx.doi.org/10.1002/grl.50704, 2013.

Rodgers, C. D.: Inverse methods for atmospheric sounding: theory and practice, vol. 2 of *Series on atmospheric, oceanic and planetary physics*, World Scientific, Singapore, River Edge, N.J., reprinted : 2004, 2008, 2000.

Schneising, O., Buchwitz, M., Reuter, M., Bovensmann, H., and Burrows, J. P.: Devastating Californian wildfires in November 2018 observed from space: the carbon monoxide perspective, Atmospheric Chemistry and Physics Discussions, 2019, 1–14, https://doi.org/10.5194/acp-2019-5, https://www.atmos-chem-phys-discuss.net/acp-2019-5/, 2019.

SMA-GDF: Inventario de Emisiones de la Ciudad de México 2016., Tech. rep., Secretaría del Medio Ambiente de la Ciudad de México: Dirección General de Gestión de la Calidad del Aire, Ciudad de México, 2018.

Spivakovsky, C. M., Logan, J. A., Montzka, S. A., Balkanski, Y. J., Foreman-Fowler, M., Jones, D. B. A., Horowitz, L. W., Fusco, A. C., Brenninkmeijer, C. A. M., Prather, M. J., Wofsy, S. C., and McElroy, M. B.: Three-dimensional climatological distribution of tropospheric OH: Update and evaluation, Journal of Geophysical Research: Atmospheres, 105, 8931–8980, https://doi.org/10.1029/1999jd901006, https://doi.org/10.1029%2F1999jd901006, 2000.

Stremme, W., Grutter, M., Rivera, C., Bezanilla, A., Garcia, A. R., Ortega, I., George, M., Clerbaux, C., Coheur, P.-F., Hurtmans, D., Hannigan, J. W., and Coffey, M. T.: Top-down estimation of carbon monoxide emissions from the Mexico Megacity based on FTIR measurements from ground and space, Atmospheric Chemistry and Physics, 13, 1357–1376, https://doi.org/10.5194/acp-13-1357-2013, https://www.atmos-chem-phys.net/13/1357/2013/, 2013.

Varon, D. J., Jacob, D. J., McKeever, J., Jervis, D., Durak, B. O. A., Xia, Y., and Huang, Y.: Quantifying methane point sources from fine-scale satellite observations of atmospheric methane plumes, Atmospheric Measurement Techniques, 11, 5673–5686, https://doi.org/10.5194/amt-11-5673-2018, https://www.atmos-meas-tech.net/11/5673/2018/, 2018.

Veefkind, J., Aben, I., McMullan, K., Förster, H., de Vries, J., Otter, G., Claas, J., Eskes, H., de Haan, J., Kleipool, Q., van Weele, M., Hasekamp, O., Hoogeveen, R., Landgraf, J., Snel, R., Tol, P., Ingmann, P., Voors, R., Kruizinga, B., Vink, R., Visser, H., and Levelt, P.: TROPOMI on the ESA Sentinel-5 Precursor: A GMES mission for global observations of the atmospheric composition for climate, air quality and ozone layer applications, Remote Sensing of Environment, 120, 70–83, https://doi.org/10.1016/j.rse.2011.09.027, https://doi.org/10.1016%2Fj.rse.2011.09.027, 2012.

Vidot, J., Landgraf, J., Hasekamp, O., Butz, A., Galli, A., Tol, P., and Aben, I.: Carbon monoxide from shortwave infrared reflectance measurements: A new retrieval approach for clear sky and partially cloudy atmospheres, Remote Sensing of Environment, 120, 255–266, https://doi.org/10.1016/j.rse.2011.09.032, https://doi.org/10.1016%2Fj.rse.2011.09.032, 2012.
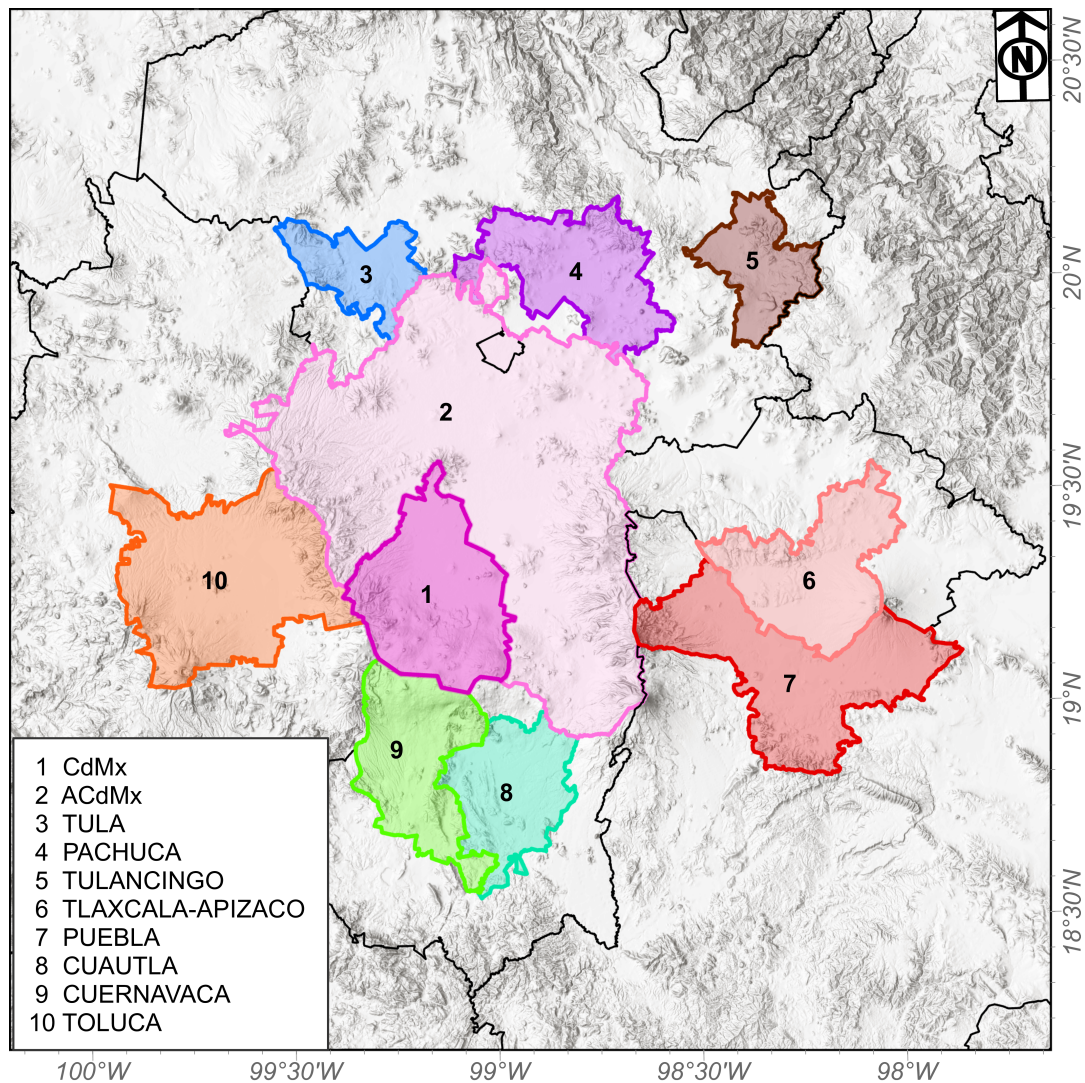
Figure 1. Urban districts surrounding Mexico City. For each of the color coded domains a separate WRF tracer run was performed based on the emissions within the polygons. The elevation map in the background is under copyright © Esri, Airbus DS, USGS, NGA, NASA, CGIAR, N Robinson, NCEAS, NLS, OS, NMA, Geodatastyrelsen, Rijkswaterstaat, GSA, Geoland, FEMA, Intermap and the GIS user community.
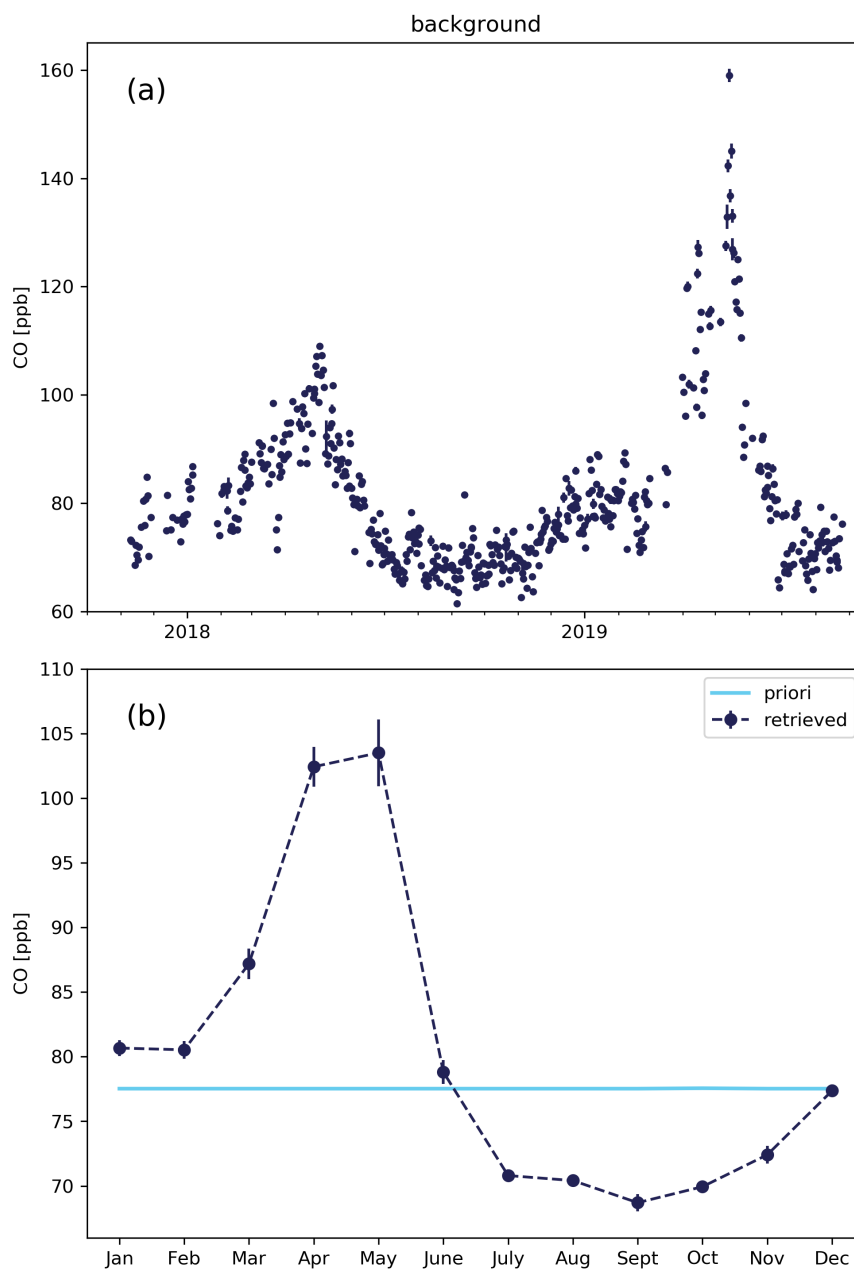
Figure 2. Background CO concentration for the domain shown in Fig. 1 estimated by fitting the WRF simulation to the TROPOMI data. (a) background CO for individual collocations from the 9th of November 2017 to the 25th of August 2019. (b) Monthly mean background CO based on the individual collocations. The error bars are the standard error of the mean and the light blue line time invariant prior used in the fit.
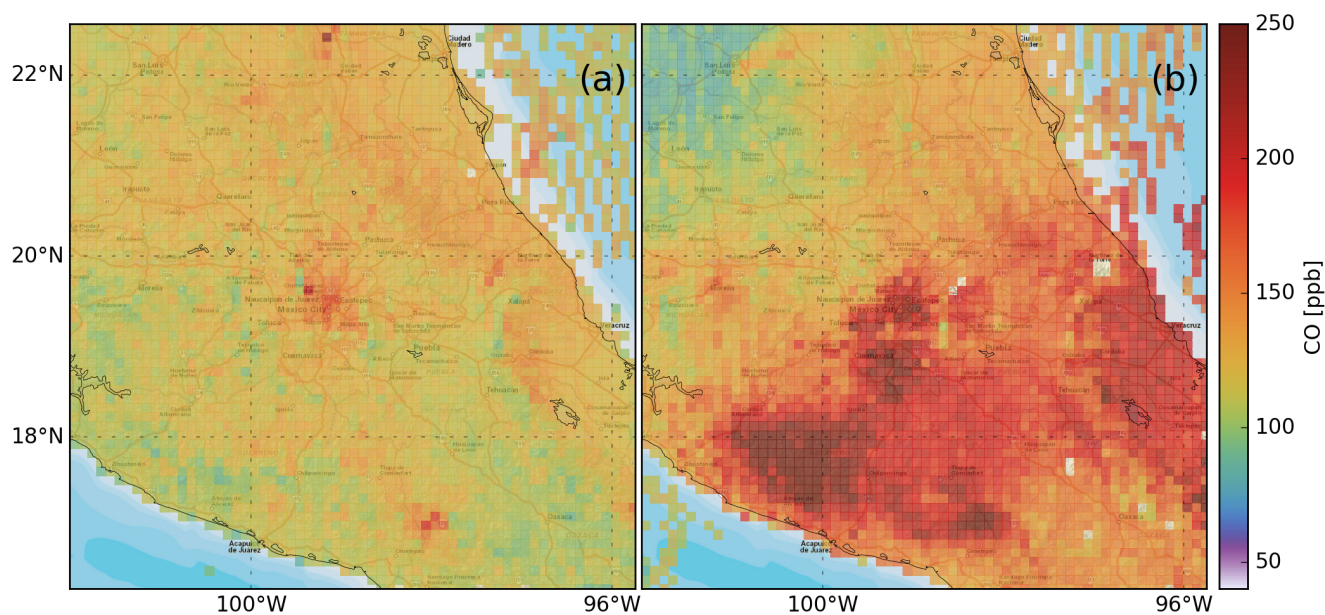
Figure 3. TROPOMI CO data over Mexico City averaged on a 0.1 by 0.1 degree lat/lon grid. (a) averaged from 12 to 18 of April 2019 showing undisturbed background CO levels. (b) averaged from 12 - 18 of May 2019 showing high CO concentrations in Mexico City caused by fires in the South-East. The street map in the background is under copyright © 2009 ESRI, AND, TANA, ESRI Japan, UNEP-WCMC.
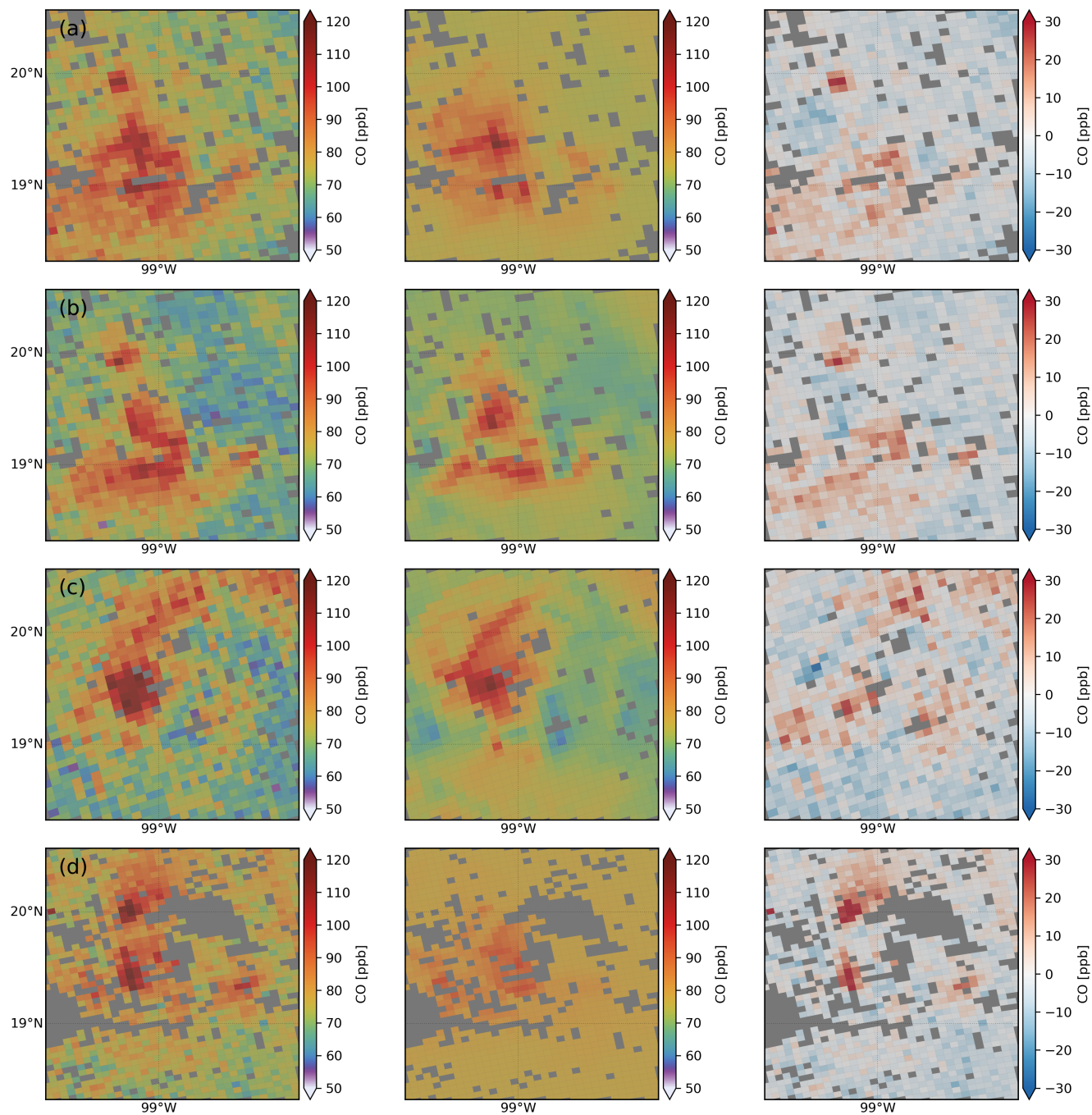
Figure 4. Example cases for fitting the WRF simulation to the TROPOMI data deploying the "Final-fit" approach for (a) the 20th of September, (b) the 7th of November, (c) the 19th of November 2018 and (d) the 17th of August 2019. TROPOMI CO retrievals (left column), WRF simulation fitted to the TROPOMI data (middle column), and the residual (right column, TROPOMI - WRF).
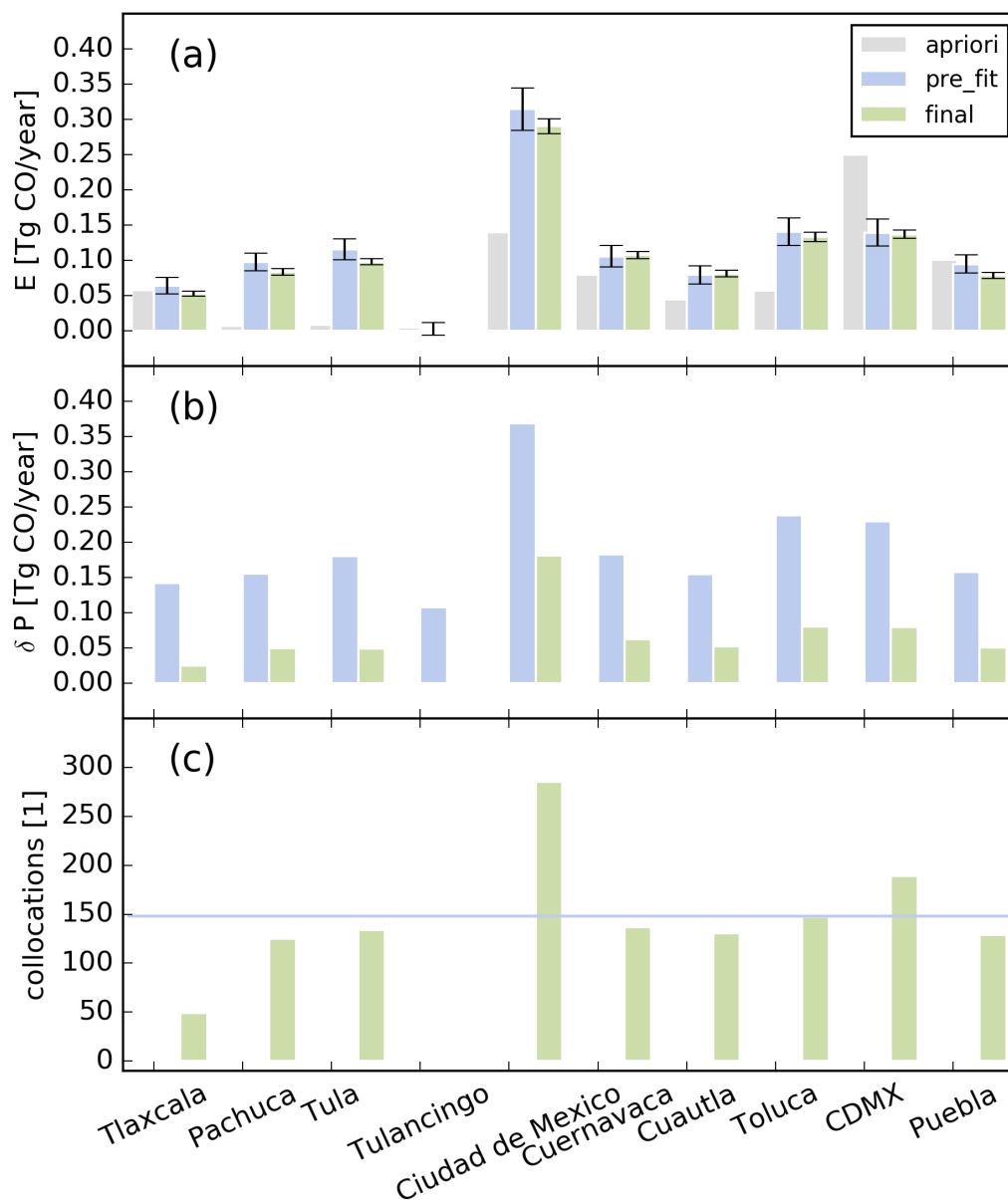
Figure 5. Statistics of CO emissions averaged from the 9th of November 2017 to the 25th of August 2019 for the tracer domains shown in Fig. 1. (a) Median of the priori emissions (adapted INEM inventory) used for the WRF simulation (grey) and retrieved from the TROPOMI data (Pre-fit in blue, Final-fit in green). The error bars indicate the standard error of the mean calculated from the delta percentiles (b) used as a robust estimation of the standard deviation and the number of collocations (c). The number of collocation of the Pre-fit is the same for all tracer domains (blue line) but in the Final-fit it is changing due to the information content filtering.
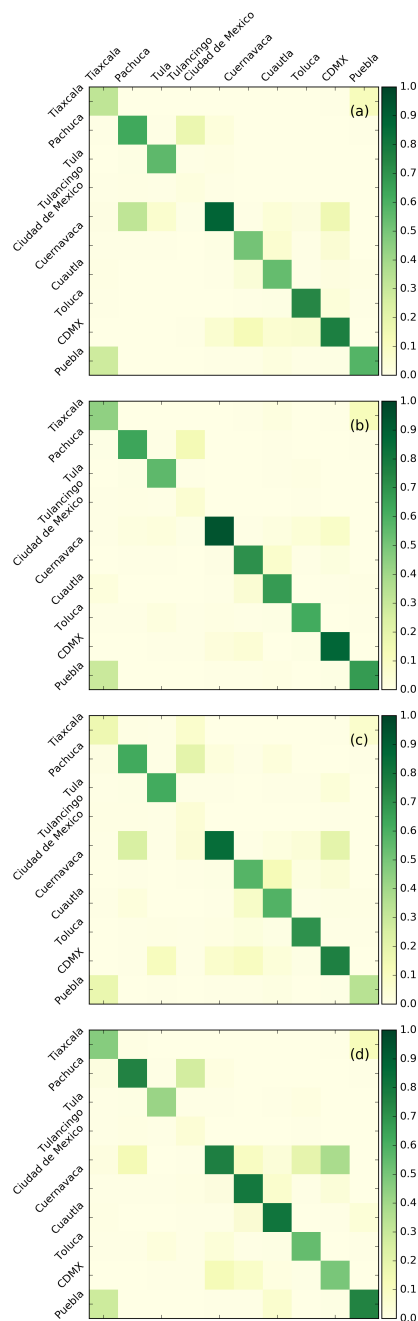
Figure 6. Averaging kernel matrices showing the sensitivity and cross-sensitivities for the scaling of the different tracer fields. The same cases as in Fig. 4 are shown for the dates (a) the 20th of September, (b) the 7th of November, (c) the 19th of November 2018 and (d) the 17th of August 2019 but deploying the regularized retrieval.
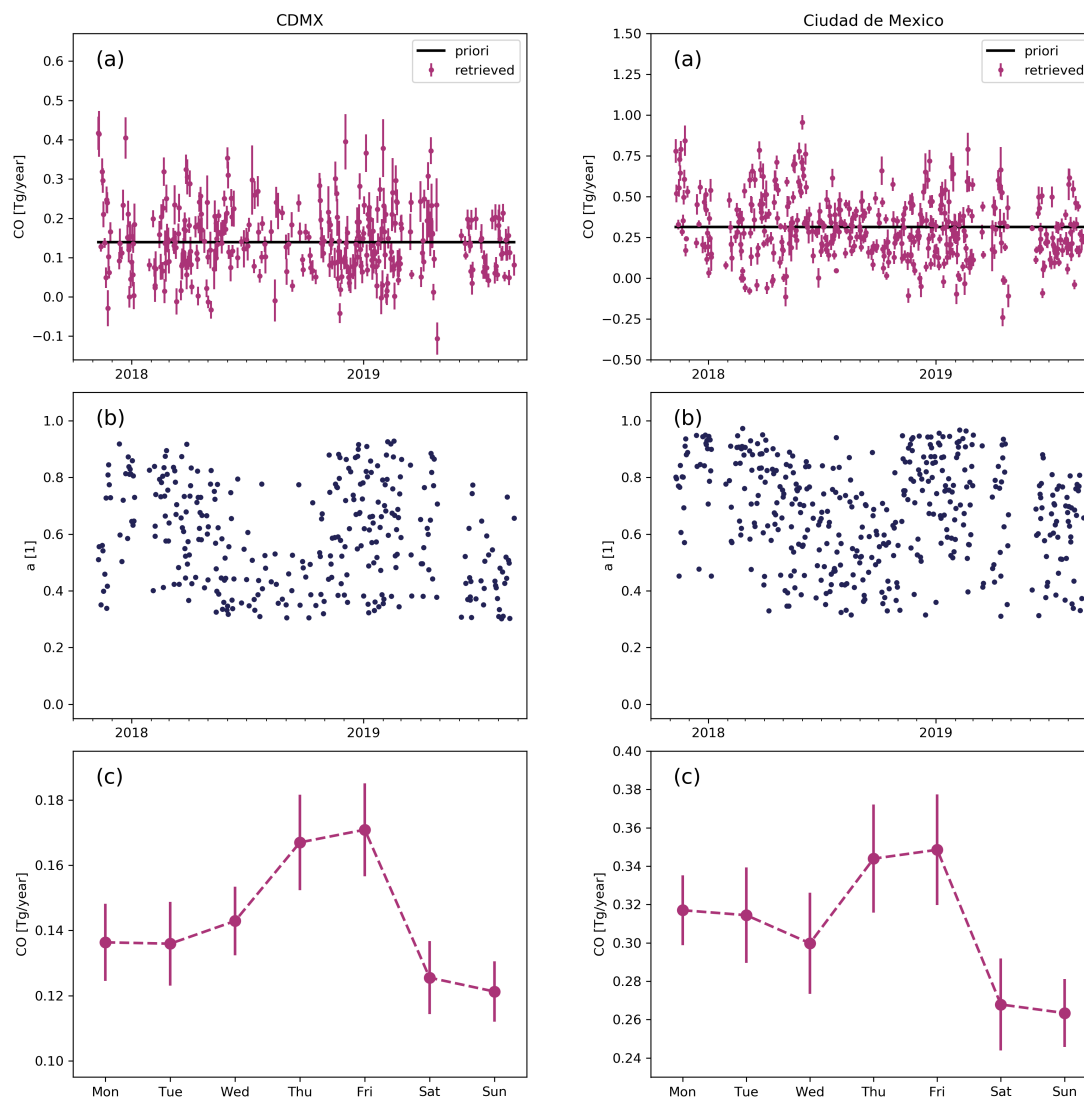
Figure 7. Retrieved CO Emissions from the TROPOMI data for the tracers CDMX (left panel) and ACDMX (right panel). (a) Time series of individual retrieved CO emissions. The error bars indicate the error of the fit and the black line is the time invariant priori used in the fit. (b) degree of freedom of the scaling factor for the tracer field. Only data with dofs > 0.3 is accounted for. (c) Weekly cycle of the CO emissions. Median values are shown and the error bars are the standard error of the mean deploying the delta percentile as a robust estimation of the standard deviation.
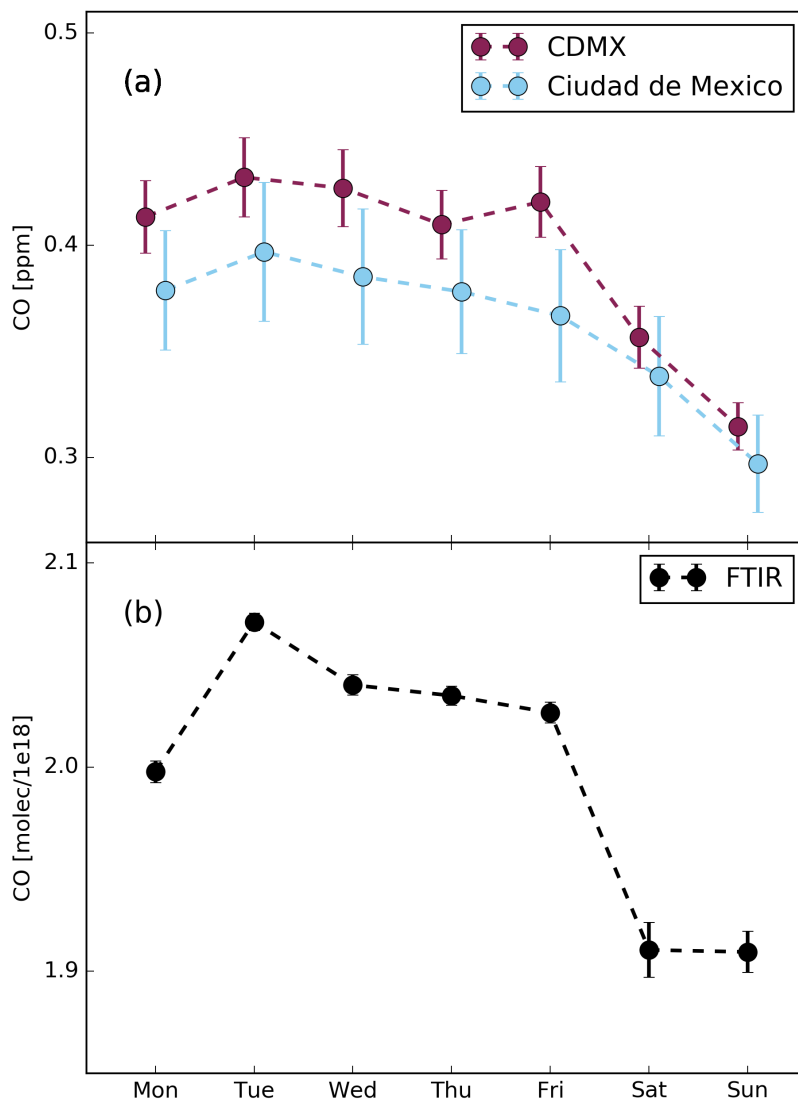
Figure 8. Weekly cycle of the CO concentration. (a) based on 29 in situ measurements station operated by SEDEMA. (b) ground-based FTIRs vertical column measurements of an instrument located in Mexico. Median values are shown and the error bars are the standard error of the mean deploying the delta percentile as a robust estimation of the standard deviation.